

Supporting Information for Mechanism of Nonmonotonic Increase in Polymer Size: Comparison between Linear and Ring Chains at High Shear Rates

Zhenhua Wang,^{†,‡} Qilong Zhai,^{†,¶} Wei Chen,[§] Xiaoliang Wang,[§] Yuyuan Lu,^{*,†}
and Lijia An^{*,†,||}

[†]*State Key Laboratory of Polymer Physics and Chemistry, Changchun Institute of Applied
Chemistry, Chinese Academy of Sciences, Changchun 130022, P.R.China*

[‡]*University of Science and Technology of China, Hefei, 230026, P.R.China*

[¶]*School of Mathematical Sciences, Peking University, Beijing 100871, P.R. China*

[§]*School of Chemistry and Chemical Engineering, Nanjing National Laboratory of
Microstructures, Nanjing University, Nanjing 210093, P.R. China*

^{||}*University of Science and Technology of China, Chinese Academy of Sciences, Hefei,
230026, P.R.China*

E-mail: yylu@ciac.ac.cn; ljan@ciac.ac.cn

Figure S1 shows the deviation from linear velocity profile of linear and nonlinear (S-shaped) flows generated by different simulation methods: (1) moving boundary walls in Slit-confined MPCD solvent (MPCD SLIT); (2) applying Lees-Edwards boundary conditions in bulk Dissipative Particle Dynamics system (DPD LEBC). It is clear that the linear flow in both cases breaks down at high shear rates.

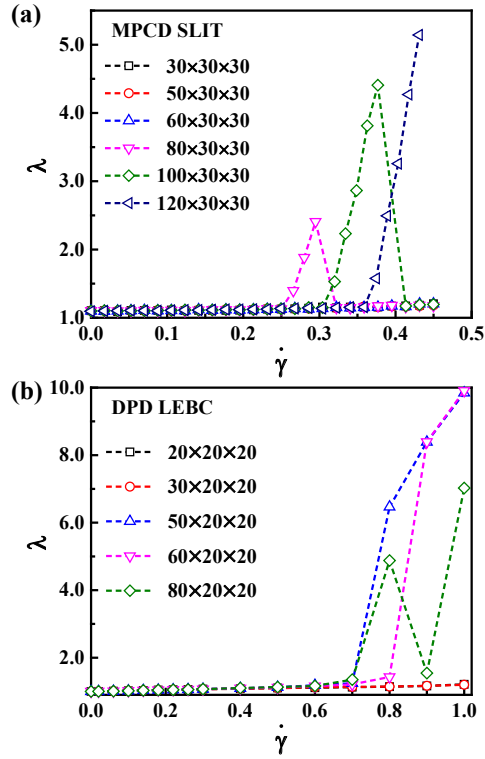


Figure S1: The transition from linear to nonlinear (S-shaped) flow in (a) MPCD SLIT and (b) DPD LEBC methods. The deviation from linear velocity profile of different flow types is characterized via $\lambda = \sum_{i=1}^n [(\mathbf{v}_{i,x} - \dot{\gamma} \mathbf{r}_{i,y})^2 + \mathbf{v}_{i,y}^2 + \mathbf{v}_{i,z}^2] / (3n)$, where n denotes the number of all particles in simulation box.

To quantify the unusual phenomena observed in the simulations, we first calculate the alignment angle, the cross-correlation function, and the end-to-end vector correlation function. These quantities reveal directly the novel dynamic behaviors of polymers at large shear rates.

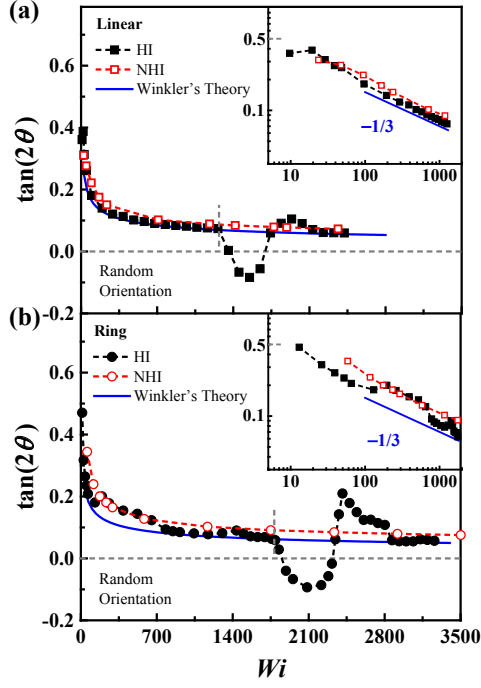


Figure S2: Dependence of $\tan(2\theta)$ on the Weissenberg number Wi for linear (a) and ring (b) polymers. The results with hydrodynamic interactions (HI) and without hydrodynamic interactions (NHI) are shown by the solid and hollow symbols, respectively. The solid blue line indicates the asymptotic dependence of Winkler's theory, $\tan(2\theta) \sim Wi^{-1/3}$.¹

Figure S2 shows the dependence of the alignment angle θ on the Weissenberg number Wi for linear and ring polymers. On the region of low shear rates, the results both with and without hydrodynamic interactions (HI and NHI) collapse approximately onto the solid blue line, in agreement with the asymptotic behaviour of Winkler's theory, $\tan(2\theta) \sim Wi^{-1/3}$.¹ This is consistent with previous studies focusing on semidilute solutions.²⁻⁶ In the weak shear regime, polymer chains stretch and recoil continuously, leading to huge conformational fluctuations. With further increasing of the shear rates, the NHI results are still in agreement with the theoretical prediction. However, depending on the shear rate and polymer topol-

ogy, the HI results deviate noticeably downward or upward from the theoretical prediction. Such deviation implies that the polymer prefers to adopt a random orientation during the tumbling motion at strong shear flows. Note that the ring polymer exhibits stronger deviation compared with the linear chains, indicating more complicated orientational behaviors. However, at extremely high shear rates, the results of both linear and ring polymers fall back to the theoretical line again, indicating a similar dynamic behavior at lower shear rate.

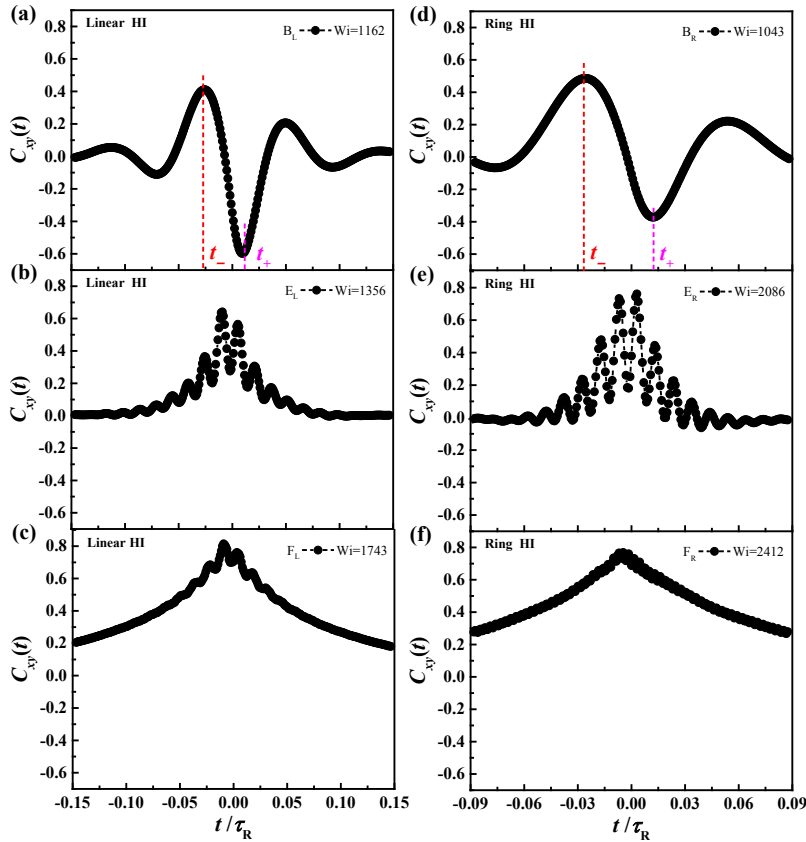


Figure S3: Cross-correlation functions for linear and ring polymers under different shear rates.

The physical origin of the tumbling motion is the successive extension and contraction of the polymer chain over time, which is induced by the coexistence of the extensional and rotational components of the simple shear flow. Traditionally, the cross-correlation $C_{xy}(t)$ between the chain extension along the flow and gradient directions was considered as an appropriate measurement of the characteristic tumbling time. As shown in Figure S3(a) and

(d), the cross-correlation function exhibits a deep minimum (less than 0) at time t_+ and a sharp peak (greater than 0) at time t_- , leading to a characteristic time for the tumbling motion, $\tau_{\text{TB}}^C = 2(t_+ - t_-)$.⁵ This behavior is observed for linear and ring polymers at small shear rates. However, at high shear rates, the negative region of the cross-correlation function $C_{xy}(t)$ disappears, accompanied by multiple oscillational peaks (as shown in Figure S3(b), (c), (e), and (f)). Thus $C_{xy}(t)$ fails to characterize the tumbling time clearly because a specific value of t_+ does not exist at all, indicating a different dynamic behavior for both linear and ring polymers under strong shear flows.

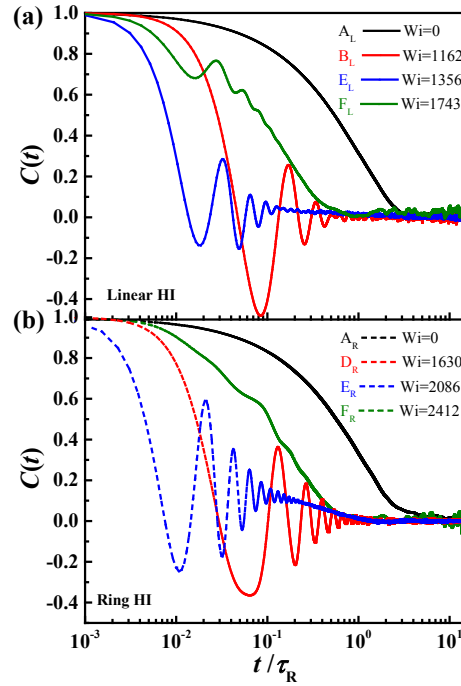


Figure S4: End-to-end vector autocorrelation functions for linear (a) and ring (b) polymers at different shear rates.

Another important function that quantifies the polymer dynamics is the normalized end-to-end vector autocorrelation function defined by $C(t) = \langle \mathbf{R}_{\text{ee}}(t) \cdot \mathbf{R}_{\text{ee}}(0) \rangle / \langle \mathbf{R}_{\text{ee}}^2 \rangle$. Here, \mathbf{R}_{ee} is the vector that connects the first and the last monomers for a linear polymer. For a ring polymer, \mathbf{R}_{ee} refers to the “diameter vector” that connects monomer pair separated by $N/2$ monomers, *i.e.*, the vector between monomer pair $(1, N/2 + 1)$. As shown in Figure

S4, for polymers at equilibrium, the autocorrelation function $C(t)$ decays exponentially. At small shear rates, the time dependence of $C(t)$ is nonmonotonic and negative regions appear. Both linear and ring polymers exhibit oscillating relaxation dynamics, confirming the existence of continuous tumbling motion. When the shear rate increases further, the polymer relaxation is dominated by the exponential relaxation again, and the negative regions no longer exist, indicating the suppression of uniform tumbling motion. Therefore, compared with the polymer dynamics in weak shear flow, large shear rates lead to a much richer variety of response behaviors for both linear and ring polymers.

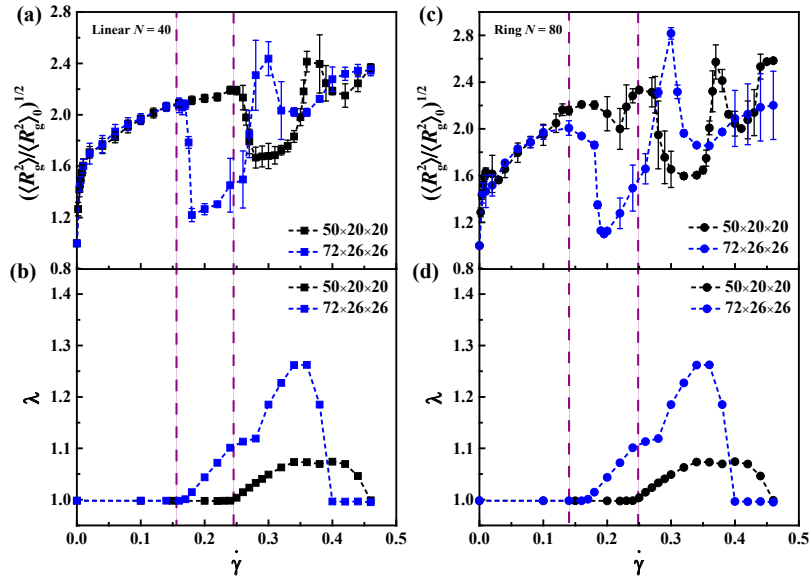


Figure S5: The corresponding relationship between the polymer size and the strength of nonlinear flow.

Figure S5 shows the corresponding relationship between the polymer size and the strength of nonlinear flow, which indicates that the nonmonotonic increase of polymer size at high shear rates is caused by the transition from linear to nonlinear (S-shaped) flow. For linear and ring polymers in a bigger simulation box ($72\sigma \times 26\sigma \times 26\sigma$, about $15.0R_{g\text{-ring}} \times 5.4R_{g\text{-ring}} \times 5.4R_{g\text{-ring}}$), the nonmonotonic dependence is detected at lower shear rate, and the Regime 4 of ring polymers disappears.

Figure S6 shows the probability distribution functions of the instantaneous radius of

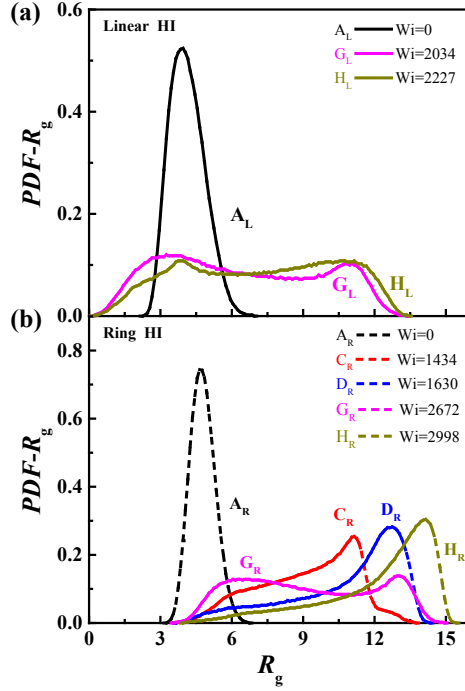


Figure S6: Probability distribution functions of the instantaneous radius of gyration R_g (PDFs- R_g) for linear (a) and ring (b) polymers at given Weissenberg numbers.

gyration R_g (PDFs- R_g) for linear and ring polymers at given Weissenberg numbers Wi . For G_L and H_L cases, the shapes of the PDFs- R_g are similar and approximately symmetric, indicating that the linear polymers undergo uniform tumbling motions. A subtle difference is that the polymer in the H_L case favors stretching conformations, leading to a larger extension than that in the G_L case. As seen from the movies, the ring polymers in the C_R , D_R , and H_R cases undergo uniform tank-treading motions, which are supported by the single peak of the PDFs- R_g . Clearly, PDF- R_g for the G_R case exhibits double peaks, corresponding to the breakdown of uniform tank-treading motion and the shrinkage of the polymer size.

Figure S7 illustrates different relatively stable stretched conformations for linear and ring polymers with the inclusion of HI at different shear rates, given by the monomer density distributions in the shear-gradient plane (a, b, c, and d) and the corresponding distribution in the shear-vorticity plane (e, f, g, and h). At large shear rate, both linear and ring polymers exhibit a *cis*-S-shaped conformation (shear-gradient plane: a and d). Due to the unique tank-

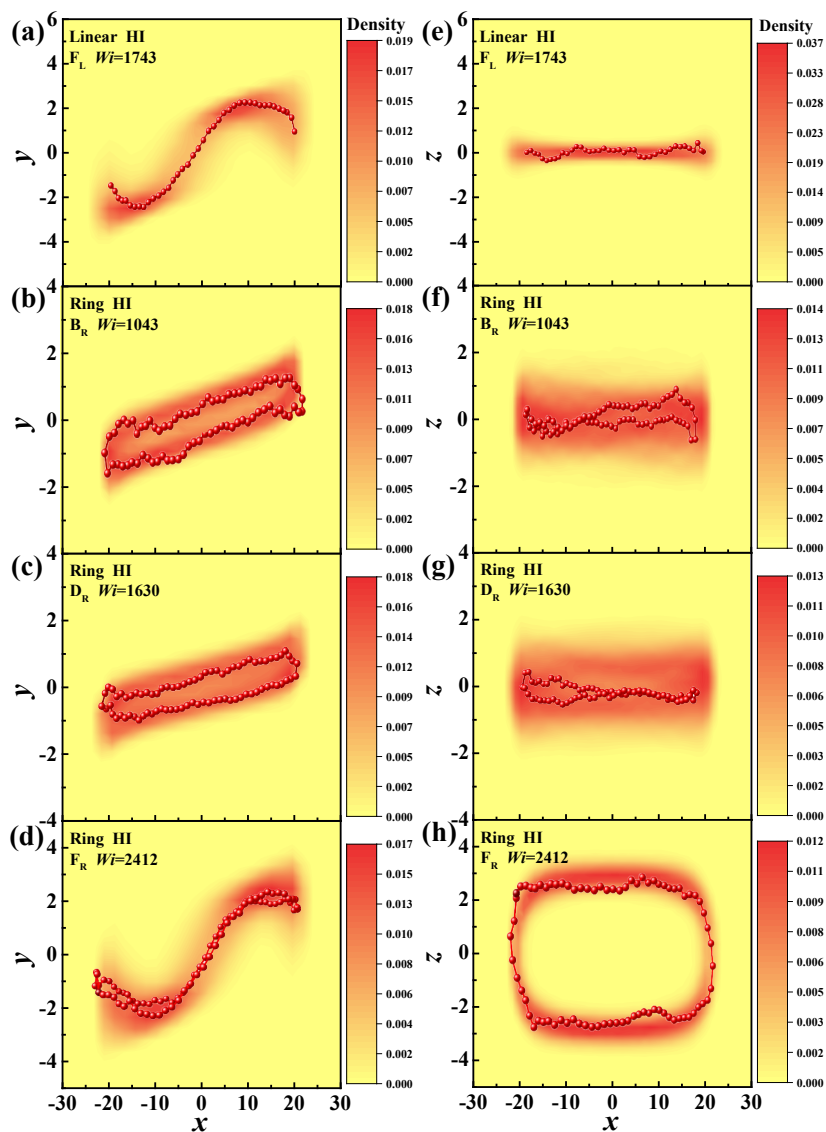


Figure S7: The monomer density distributions of stretched conformations for linear and ring polymers at large shear rates with the inclusion of HI.

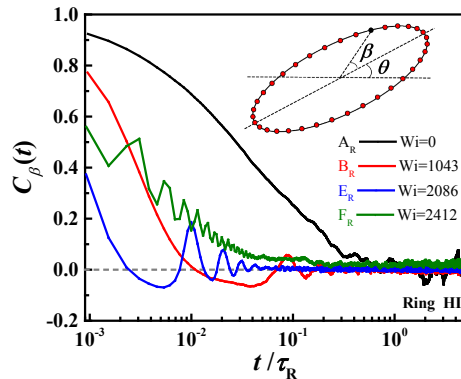


Figure S8: The angular autocorrelation functions for ring polymers at given shear rates.

treading motion, the ring polymer exhibits another relatively stable stretched state with an oval conformation at moderate shear rates (shear-gradient plane: b and c).

As shown in the B_R case in Figure S8, a second peak of the angular autocorrelation function appears at half of the characteristic time for tank-treading motion. In the E_R case, the ring polymer collapses to a coil-like conformation, supported by the remarkable decrease of the average polymer size. Moreover, it can be seen from the polymer trajectories in SI-movie 11 that the polymer chain exhibits a rapid rotation without significantly changing its collapsed shape. In other words, the tank-treading motion has been largely suppressed by the shear flow in the E_R case, because the extended conformations no longer exist. However, the angular autocorrelation function for the E_R case in Figure S8 indicates a uniform tank-treading motion rather than the suppressed behavior, leading to an inappropriate prediction in the large shear regime.

Movies

Trajectories of linear and ring polymers at different Weissenberg numbers in their respective mass center coordinates. Two half parts of the polymer beads are labeled with different colors for visualization. All movies generated by VMD⁷ are as follows:

SI-movie 1: Linear chain at equilibrium (A_L case).

SI-movie 2: Linear chain under shear flow at $Wi = 1162$ (B_L case).
SI-movie 3: Linear chain under shear flow at $Wi = 1356$ (E_L case).
SI-movie 4: Linear chain under shear flow at $Wi = 1743$ (F_L case).
SI-movie 5: Linear chain under shear flow at $Wi = 2034$ (G_L case).
SI-movie 6: Linear chain under shear flow at $Wi = 2227$ (H_L case).
SI-movie 7: Ring chain at equilibrium (A_R case).
SI-movie 8: Ring chain under shear flow at $Wi = 1043$ (B_R case).
SI-movie 9: Ring chain under shear flow at $Wi = 1434$ (C_R case).
SI-movie 10: Ring chain under shear flow at $Wi = 1630$ (D_R case).
SI-movie 11: Ring chain under shear flow at $Wi = 2086$ (E_R case).
SI-movie 12: Ring chain under shear flow at $Wi = 2412$ (F_R case).
SI-movie 13: Ring chain under shear flow at $Wi = 2672$ (G_R case).
SI-movie 14: Ring chain under shear flow at $Wi = 2998$ (H_R case).

References

- (1) Winkler, R. G. Conformational and rheological properties of semiflexible polymers in shear flow. *J. Chem. Phys.* **2010**, 133, 164905.
- (2) Huang, C.-C.; Sutmann, G.; Gerhard, G.; Roland, G. W. Tumbling of polymers in semidilute solution under shear flow. *Europhys. Lett.* **2011**, 93, 54004.
- (3) Huang, C.-C.; Winkler, R. G.; Sutmann, G.; Gompper, G. Semidilute polymer solutions at equilibrium and under shear flow. *Macromolecules* **2010**, 43, 10107-10116.
- (4) Fedosov, D. A.; Singh, S. P.; Chatterji, A.; Winkler, R. G.; Gompper, G. Semidilute solutions of ultra-soft colloids under shear flow. *Soft Matter* **2012**, 8, 4109-4120.
- (5) Huang, C.-C.; Gompper, G.; Winkler, R. G. Non-equilibrium relaxation and tumbling times of polymers in semidilute solution. *J. Phys.: Condens. Matter* **2012**, 24, 284131.

- (6) Singh, S. P.; Chatterji, A.; Gompper, G.; Winkler, R. G. Dynamical and rheological properties of ultrasoft colloids under shear flow. *Macromolecules* **2013**, 46, 8026-8036.
- (7) Humphrey, W.; Dalke, A.; Schulten, K. VMD: Visual Molecular Dynamics. *J. Mol. Graph.* **1996**, 14, 33-38.